A FORMULATION FOR THE ANALYSIS OF PELLET-CLADDING MECHANICAL INTERACTION

Y. Y. LIU

Materials Science Division, Argonne National Laboratory, 9700 South Cass Avenue, Argonne, Illinois 60439, U.S.A.

J. E. MEYER, A. S. ARGON

Department of Nuclear Engineering, Massachusetts Institute of Technology, Cambridge, Massachusetts 02139, U.S.A.

SUMMARY

A formulation has been derived for the thermoelastic analysis of pellet-cladding mechanical interaction. The formulation is based on a combination of finite element analysis and the matrix-displacement method. Boundary conditions at the pellet-cladding and pellet-pellet contacting sites can be treated realistically by considering the force and displacement relationships at the interfaces. As a result, no simulating gap elements need be used and the analysis of the two limiting cases, fuel-cladding bonding (stick) and fuel-cladding slippage (slip), follows directly from imposing the appropriate boundary conditions. From the principle of superposition, this formulation also gives a very compact scheme which can be used to study a variety of power ramp cases with ease. No additional finite element analysis is required after the solutions for a number of individual base-case problems have been obtained.

Because the thermoelastic response of a fuel-element during a power ramp corresponds to that for a fast ramp rate, which subjects cladding to the most severe mechanical loading, the results from our thermoelastic analysis can be very useful in evaluating the likelihood of cladding failure when they are combined with knowledge of the cladding failure mode (plastic instability or stress-corrosion cracking). Since the failure mode for the Light Water Reactor fuel elements is predominantly stress-corrosion cracking and there is generally no time-independent cladding plastic deformation during a power ramp, our formulation may be applied directly to provide an assessment of the permissible power ramps. This could lead to a relaxation of the current restrictive and empirically based reactor-operation rules.

*Work supported by the U.S. Department of Energy.

1. Introduction

Pellet-cladding interaction (PCI), a term which generally includes both mechanical and chemical interactions between fuel pellet and cladding, is the major midlife failure mechanism for cylindrical fuel elements after the fuel-cladding gap has closed during irradiation. The failures normally occur after rapid up-power excursions (ramps), and the failure sites are almost invariably located at pellet-pellet interfaces, spatially associated with the circumferential ridges formed on the cladding outer surface. The cladding failure can be due either to loss of ductility caused by neutron irradiation, or to stress-corrosion cracking in which chemical attack by fission products also plays a role. In both cases, the main source of the mechanical load on cladding is the differential thermal expansion of fuel and cladding during a power ramp.

Because the ramp failures are highly localized, conventional analysis based on the assumption of generalized plane strain is not suitable. The prevalent approach in current two- and three-dimensional finite element fuel-behavior analyses relies on the use of simulating elements for pellet-cladding gap and pellet-pellet interfaces. For example, both Levy and Wilkinson [1] and Rashid [2] have used mathematical springs and uniaxial contact elements in their analyses. These fictitious elements generally possess a unique stress-strain property such that either a very small or a very large elastic modulus can be employed, depending upon whether a specified strain breakpoint in the element is exceeded or not. The values of these parameters (initial and final elastic moduli and strain breakpoint) must all be assigned by the analyst, with or without proper justifications. Furthermore, there is a possibility that element rotation can occur and the strain in such elements may never become large enough to exceed the strain breakpoint. In the case of the two-dimensional elastic, orthotropic, layer-elements used by Rand et al. [3], the situation is similar in that the values of the direction-dependent elastic moduli of the simulating elements must be assigned.

In the present paper, we shall derive a formulation for the thermoelastic analysis of pellet-cladding mechanical interaction. The formulation is based on a combination of finite element analysis and the matrix-displacement method. Boundary conditions at the pellet-cladding and pellet-pellet contacting sites can be treated realistically by considering the force and displacement relationships at the interfaces. As a result, no simulating elements need be used and the analysis of the limiting cases, fuel-cladding bonding (stick) and fuel-cladding slippage (slip), follows directly from imposing the appropriate boundary conditions.

2. Formulation

Figure 1 shows an idealized picture of a portion of the pellet-cladding contact configuration. We assume that the number of identical pellets both above and below the ones shown in Figure 1 is sufficient that this figure can be regarded as representative. From symmetry considerations, this portion can be further reduced to only one quarter of a pellet and the associated cladding sector, as shown in Figure 2. The parameters in Figure 2 have the following meanings:

- T_p, T_c: temperature distributions of pellet and cladding, respectively
- P_i: fuel-rod internal pressure (the sum of the pressures due to fission gas and prepressurization, if any)

P_o: external coolant pressure

F_c: interfacial normal contacting force

F_T: interfacial shear contacting force

$F_A{}^p, F_A{}^c$: axial forces on pellet and cladding top ends

Among the various thermal and mechanical loadings on the pellet and cladding, the internal and external pressures and the temperature gradients can be handled easily in the analysis of deformation and stresses. The determination of the forces at the pellet-cladding and pellet-pellet interfaces, however, involves mixed boundary conditions in which both force and displacement must be considered at these contacting sites. At the pellet-pellet interface, a further complication arises from the consideration that the region near which the axial forces are acting will deform, changing the contacting area between pellets. In our formulation, the pellet-pellet interface condition is treated by adapting the classical Hertz solution for two spherical bodies in contact [4] as follows:

$$a = (3F_A R_o / 4E_o)^{1/3} \tag{1}$$

where a is the radius of the circular contact area between pellets: F_A is the axial force related to the pressure distribution, P, as assumed by Hertz:

$$P = P_o(1 - r^2/a^2)^{1/2} \tag{2}$$

with

$$P_o = 3F_A/2\pi a^2 \ , \tag{3}$$

and

$$R_o = 1/2 \ R_p \ , \tag{4}$$

$$E_o = \frac{E_p}{2(1 - \nu_p{}^2)} \tag{5}$$

where

where R_p, E_p, and ν_p are the radius of curvature, Young's modulus and the Poisson ratio of the fuel pellet, respectively.

The radius of curvature at the pellet top end due to thermal hourglassing has been determined previously [5] and is usually 40-50 times larger than the pellet radius. To determine the value of a from Eq. (1), one needs to know the magnitude of $F_A{}^p$. However, $F_A{}^p$ cannot be found until the entire problem is solved. A rigorous solution therefore requires iteration until the answers converge. This iteration scheme was not adopted by the present authors; instead, a few trial cases were computed with different values of F_A to determine the corresponding radius of the contacting area. At an assumed fuel centerline temperature of 2,000°C at which E_p and ν_p values were evaluated, we found that the radius of the contacting area is small under the gravity loading from a stack of 100 pellets. Furthermore, 'a' changes only by a factor of two when F_A is increased by a factor of ten. We have therefore chosen a small but finite contacting area over the pellet top end (a = 0.4 mm) as shown in Figure 2.

After the size of the contacting area is assigned, the problem illustrated in Figure 2 can be solved by a combination of finite element analysis and the matrix displacement method using the principle of superposition.

Figures 3 and 4 illustrate how the superposition principle is applied to this problem; in these figures, the loadings shown in Figure 2 for pellet and cladding have been separated into individual base-case problems (8 for pellet and 9 for cladding). For thermoelastic analysis with constant material properties (obtained at volume-averaged fuel and cladding temperatures), the overall solution for the problem shown in Figure 2 can be obtained by summing the solutions of the individual cases, provided that F_C, F_T, and F_A are all known.

Mathematically, the displacements at any point in the pellet and cladding from the combined loadings can be written as

$$\begin{bmatrix} u \\ w \end{bmatrix}^p = \begin{bmatrix} u \\ w \end{bmatrix}^p_{q'} + \begin{bmatrix} u \\ w \end{bmatrix}^p_{T_{ps}} + \begin{bmatrix} u \\ w \end{bmatrix}^p_{P_i} + \begin{bmatrix} u \\ w \end{bmatrix}^p_{F_C} + \begin{bmatrix} u \\ w \end{bmatrix}^p_{F_T} + \begin{bmatrix} u \\ w \end{bmatrix}^p_{F_{A,1}} + \begin{bmatrix} u \\ w \end{bmatrix}^p_{F_{A,2}} + \begin{bmatrix} u \\ w \end{bmatrix}^p_{F_{A,3}} \tag{6}$$

and

$$\begin{bmatrix} u \\ w \end{bmatrix}^c = \begin{bmatrix} u \\ w \end{bmatrix}^c_{q'} + \begin{bmatrix} u \\ w \end{bmatrix}^c_{T_{cs}} + \begin{bmatrix} u \\ w \end{bmatrix}^c_{P_i} + \begin{bmatrix} u \\ w \end{bmatrix}^c_{P_o} + \begin{bmatrix} u \\ w \end{bmatrix}^c_{F_C} + \begin{bmatrix} u \\ w \end{bmatrix}^c_{F_T} + \begin{bmatrix} u \\ w \end{bmatrix}^c_{F_{A,4}} + \begin{bmatrix} u \\ w \end{bmatrix}^c_{F_{A,5}} + \begin{bmatrix} u \\ w \end{bmatrix}^c_{F_{A,6}} \tag{7}$$

where u and w are the radial and axial displacements, superscripts p and c refer to pellet and cladding, respectively, and the other symbols are identified with the individual cases shown in Figures 3 and 4.

Notice that the displacements due to temperature distributions in pellet and cladding have been separated into two terms. The first term on the right side of Eq. (6) or Eq. (7) gives the displacements from the fuel-element linear heat rating, q', evaluated at zero surface temperature, whereas the second term on the right side of the above equations gives the displacements from uniform thermal expansion up to the corresponding surface temperatures. For the cladding the displacements from uniform thermal expansion can be written as

$$\begin{bmatrix} u \\ w \end{bmatrix}^{c}_{T_{cs}} = \alpha_c [T_{cs} - T_R] \begin{bmatrix} r \\ z \end{bmatrix}_c \tag{8}$$

where α_c is the cladding thermal expansion coefficient and T_{cs} and T_R are, respectively, the cladding inner-surface temperature and the reference temperature.

The equation for the pellet displacements due to uniform thermal expansion is obtained similarly as

$$\begin{bmatrix} u \\ w \end{bmatrix}^{p}_{T_{ps}} = \alpha_p [T_{ps} - T_R] \begin{bmatrix} r \\ z \end{bmatrix}_p \tag{9}$$

where α_p is the fuel thermal expansion coefficient obtained at the pellet outer-surface temperature, T_{ps}.

The separation of temperature distributions into two terms offers an advantage in that q' and the surface temperatures can be varied independently. This greatly increases the number of power-ramp cases which can be studied by applying the superposition principle.

To obtain solutions for the individual base-case problems, we perform a finite element analysis for each case with a specified reference loading of unit magnitude. Each case then provides a column vector which relates the displacements of interest to the specified unit reference load. The displacements of interest for the particular case shown in Figure 2 are at the points 1, 2, and 3 for the pellet; 4, 5, and 6 for the cladding; and at the pellet-cladding contacting point 'I'. The displacements and the forces at these points are related by

$$\begin{bmatrix} \tilde{u} \\ \tilde{w} \end{bmatrix}^{p} = \begin{bmatrix} \tilde{u} \\ \tilde{w} \end{bmatrix}^{p}_{sub} + \left[\begin{matrix} \tilde{u} \\ \tilde{w} \end{matrix}\Bigg|_{F_C} \quad \begin{matrix} \tilde{u} \\ \tilde{w} \end{matrix}\Bigg|_{F_T} \quad \begin{matrix} \tilde{u} \\ \tilde{w} \end{matrix}\Bigg|_{F_{A,1}} \quad \begin{matrix} \tilde{u} \\ \tilde{w} \end{matrix}\Bigg|_{F_{A,2}} \quad \begin{matrix} \tilde{u} \\ \tilde{w} \end{matrix}\Bigg|_{F_{A,3}} \right]^{p} [F]^{p} \tag{10}$$

$$\begin{bmatrix} \tilde{u} \\ \tilde{w} \end{bmatrix}^{c} = \begin{bmatrix} \tilde{u} \\ \tilde{w} \end{bmatrix}^{c}_{sub} + \left[\begin{matrix} \tilde{u} \\ \tilde{w} \end{matrix}\Bigg|_{F_C} \quad \begin{matrix} \tilde{u} \\ \tilde{w} \end{matrix}\Bigg|_{F_T} \quad \begin{matrix} \tilde{u} \\ \tilde{w} \end{matrix}\Bigg|_{F_{A,4}} \quad \begin{matrix} \tilde{u} \\ \tilde{w} \end{matrix}\Bigg|_{F_{A,5}} \quad \begin{matrix} \tilde{u} \\ \tilde{w} \end{matrix}\Bigg|_{F_{A,6}} \right]^{c} [F]^{c} \tag{11}$$

where

$$\begin{bmatrix} \tilde{u} \\ \tilde{w} \end{bmatrix}^{p\,T} = [u_I^{\,p}\ w_I^{\,p}\ w_1^{\,p}\ w_2^{\,p}\ w_3^{\,p}]$$

$$\begin{bmatrix} \tilde{u} \\ \tilde{w} \end{bmatrix}^{c\,T} = [u_I^{\,c}\ w_I^{\,c}\ w_4^{\,c}\ w_5^{\,c}\ w_6^{\,c}]$$

$$\{[F]^p\}^T = [F_C \; F_T \; F_{A,1} \; F_{A,2} \; F_{A,3}]^p$$

$$\{[F]^c\}^T = [F_C \; F_T \; F_{A,4} \; F_{A,5} \; F_{A,6}]^c$$

and

$$\begin{bmatrix} \underset{\sim}{u} \\ \underset{\sim}{w} \end{bmatrix}^p_{sub} = \begin{bmatrix} \underset{\sim}{u} \\ \underset{\sim}{w} \end{bmatrix}^p_{q'} + \begin{bmatrix} \underset{\sim}{u} \\ \underset{\sim}{w} \end{bmatrix}^p_{T_{ps}} + \begin{bmatrix} \underset{\sim}{u} \\ \underset{\sim}{w} \end{bmatrix}^p_{P_i}$$

$$\begin{bmatrix} \underset{\sim}{u} \\ \underset{\sim}{w} \end{bmatrix}^c_{sub} = \begin{bmatrix} \underset{\sim}{u} \\ \underset{\sim}{w} \end{bmatrix}^c_{q'} + \begin{bmatrix} \underset{\sim}{u} \\ \underset{\sim}{w} \end{bmatrix}^c_{T_{cs}} + \begin{bmatrix} \underset{\sim}{u} \\ \underset{\sim}{w} \end{bmatrix}^c_{P_i} + \begin{bmatrix} \underset{\sim}{u} \\ \underset{\sim}{w} \end{bmatrix}^c_{P_o}$$

By using the appropriate boundary conditions, Eqs. (10) and (11) can be solved for the following two cases:

1. Fuel-Cladding Bonding

In the case of fuel-cladding bonding, there is no relative displacement between pellet and cladding at the contacting point; therefore,

$$u_I^p = u_I^c; \; w_I^p = w_I^c \tag{12}$$

The equilibrium of interfacial contacting forces requires

$$|F_C|^p = |F_C|^c$$

$$|F_T|^p = |F_T|^c \tag{13}$$

The axial boundary conditions at the pellet top end are such that the pellet center region defined by the radius of the contacting area remains flat and the new position of the tangent plane from the pellet center remains a symmetry plane. These conditions are schematically illustrated in Figure 5, with planes 1 and 2 corresponding to the symmetry planes before and after the power ramp, respectively. With these additional conditions, we have

$$w_1^p = w_2^p = w_3^p = w_4^c = w_5^c = w_6^c \, , \tag{14}$$

and the summation of the axial forces across the symmetry plane must be equal to zero:

$$\sum_i F_{A,i} = 0, \quad i = 1,2,3,4,5,6 \tag{15}$$

Utilizing the conditions given in Eqs. (12)-(15), Eqs. (10) and (11) can be solved by matching the proper displacement terms. A simple matrix inversion then gives all the unknowns in $[F]^P$ and $[F]^C$.

2. <u>Fuel-Cladding Slippage</u>

In the case where the limiting frictional force is reached, the conditions at the pellet-cladding contacting point become

$$u_I^{\ P} = u_I^{\ C}; \ w_I^{\ P} \neq w_I^{\ C} \tag{16}$$

$$|F_C|^P = |F_C|^C$$

$$|F_T|^P = |F_T|^C = \mu|F_C|^P = \mu|F_C|^C \tag{17}$$

where μ is the coefficient of friction between the pellet and cladding.

The axial boundary conditions in this case are

$$w_1^{\ P} = w_2^{\ P} = w_3^{\ P} ,$$

$$w_4^{\ C} = w_5^{\ C} = w_6^{\ C} \tag{18}$$

and

$$F_A^{\ P} = \sum_{i=1}^{3} F_{A,i}^P = \frac{1}{2} b^2 \ P_i - \mu F_C \tag{19}$$

$$F_A^{\ C} = \sum_{i=4}^{6} F_{A,i}^C = \frac{1}{2} (r_i^{\ 2} P_i - r_o^{\ 2} P_o) + \mu F_C \tag{20}$$

where b is the pellet radius, r_i and r_o are the cladding inner and outer radii, and the forces are balanced for a 1-radian segment of an axisymmetric, cylindrical fuel rod.

Utilizing the conditions given in Eqs. (16) to (20), Eqs. (10) and (11) can be solved in a manner similar to that for the fuel-cladding bonding case. Notice that the resulting $[F]^P$ and $[F]^C$ from the solution of these equations are the correct load fractions with respect to the specified unit reference loads in the individual base-case problems. The desired forces can be obtained by multiplying these correct load fractions by the unit reference loads.

Detailed local stress and strain distributions in the pellet and cladding can be found from the correct load fractions and the corresponding stress and strain distributions in the base-case problems, again by simple multiplication and summation. The superposition principle is therefore being applied <u>twice</u> in the present context. It is applied first to separate the combined loadings into individual base cases and to obtain force-displacement flexibility matrices for pellet and cladding, respectively. After the unknown forces are solved in terms of the correct load fractions with respect to the unit reference loads, the superposition principle is applied again to obtain the stress and strain distributions. The advantage of this method is that it gives a very compact formulation which can be used to investigate a variety of power-ramp cases with ease. No additional finite element analysis is required after the solutions for the individual base-case problems have been obtained.

3. Results

A number of power-ramp cases for the Light Water Reactor fuel elements have been analyzed using the above formulations. Typically, the cladding stresses and strains are highly localized near the pellet-cladding contacting site under the fuel-cladding bonding condition, but they are smoothed out considerably when fuel-cladding slippage occurs. Figure 6 shows a comparison of the cladding tangential stresses, $\sigma_{\theta\theta}$, under fuel-cladding bonding and with two different friction coefficients at the pellet-cladding interface. $\sigma_{\theta\theta}$ is the maximum principal stress near the cladding inner surface and is tensile in nature. The power ramp in this case corresponds to a setp power increase with a ramp magnitude of 23 kW/m (7 kW/ft). It is evident that the selected friction coefficients (μ = 0.5 and μ = 0.1) have a rather large effect in reducing the magnitude of the cladding local stresses as compared to the effect obtained under fuel-cladding bonding conditions. The other stress components exhibit similar trends; the details of those results as well as of other power-ramp cases have been given elsewhere [6].

4. Conclusions

Because the thermoelastic response of a fuel element during a power ramp corresponds to that for a fast ramp rate, which subjects cladding to the most severe mechanical loading, the results from our thermoelastic analysis can be very useful in evaluating the likelihood of cladding failure when they are combined with knowledge of the cladding failure mode (plastic instability or stress-corrosion cracking). Since the failure mode for the Light Water Reactor fuel-elements is predominantly stress-corrosion cracking and there is generally no time-independent cladding plastic deformation during a power ramp, our formulation may be applied directly to provide an assessment of the permissible power ramps. This could lead to a relaxation of the current restrictive and empirically based reactor-operation rules.

References

[1] LEVY, S. and WILKINSON, J. P. D., "A Three-Dimensional Study of Nuclear Fuel Rod Behavior During Start-up," Second Intl. Conf. on Structural Mechanics in Reactor Technology, Berlin, Germany, September 10-14, 1973, Vol. 1, Part D, D 1/5.

[2] RASHID, Y. R., "Mathematical Modeling and Analysis of Fuel Rods," Nucl. Eng. Des., 29, 22-32 (1974).

[3] RAND, R. A., et al., "A Study of Strain Distributions in Stainless Steel Fuel Rod Cladding," Third Intl. Conf. on Structural Mechanics in Reactor Technology, London, United Kingdom, September 1-5, 1975, Vol. 1, Part C, C 2/3.

[4] JONES, D. E. and SCHOTT, G. A., "English Trans. of H. Hertz, Miscellaneous Papers," Macmillan, New York (1896), 146-162 and 163-183.

[5] LIU, Y. Y., MEYER, J. E., and ARGON, A. S., "Design of Pellet Geometry to Minimize Pellet-Cladding Mechanical Interaction," submitted to Nucl. Technol., January 1979.

[6] LIU, Y. Y., "A Mechanistic Study of Light Water Reactor Fuel Element Failures," D. Sc. thesis, Nucl. Eng. Dept., Massachusetts Institute of Technology, February 1978.

Acknowledgments

The authors gratefully acknowledge the financial support provided through the MIT Energy Laboratory by Northeast Utilities Service Company, Yankee Atomic Electric Company, New England Electric System and Public Service Electric and Gas Company (N.J.) during the research period, and the support (YYL) of the U.S. Department of Energy during the writing of this manuscript. Thanks (YYL) are also expressed to Dr. F. A. Nichols for his technical comments and to Dr. E. M. Stefanski for editing the manuscript.

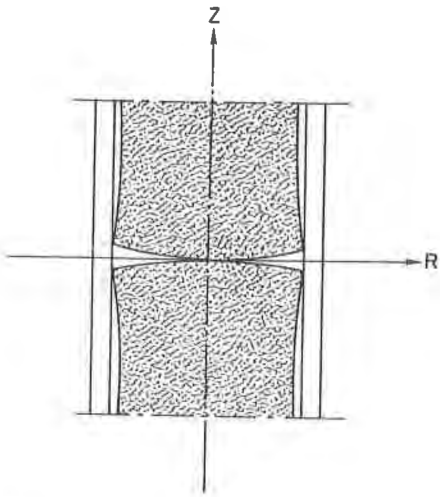

1. Schematic diagram showing the symmetrical portion of pellet-cladding contact configuration. Neg. No. MSD-65948.

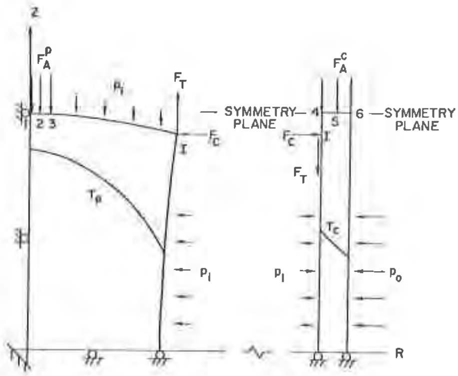

2. Schematic diagram showing the thermal/mechanical loads on pellet and cladding. Neg. No. MSD-65949.

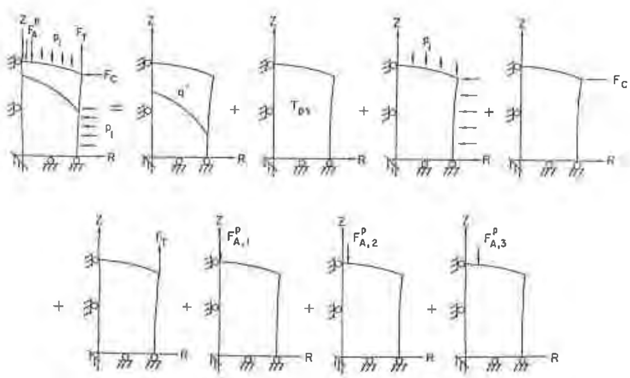

3. Individual base-case problems for pellet, illustrating principle of superposition. Neg. No. MSD-65951.

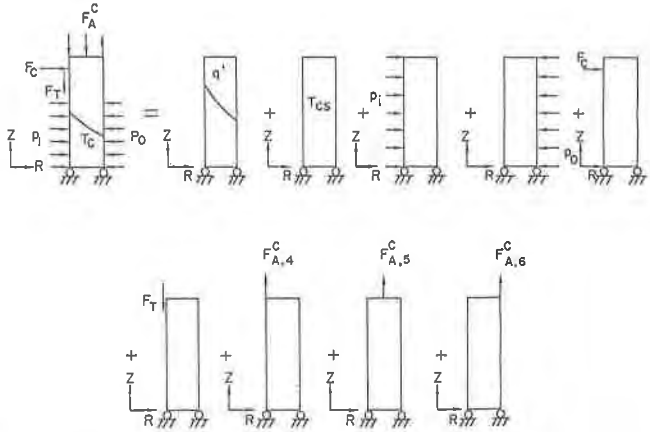

4. Individual base-case problems for cladding, illustrating principle of superposition. Neg. No. MSD-65952.

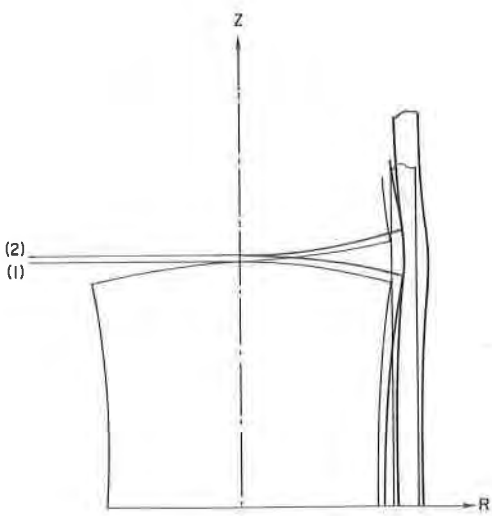

5. Schematic diagram showing the pellet-cladding contact configuration during and after a power ramp.

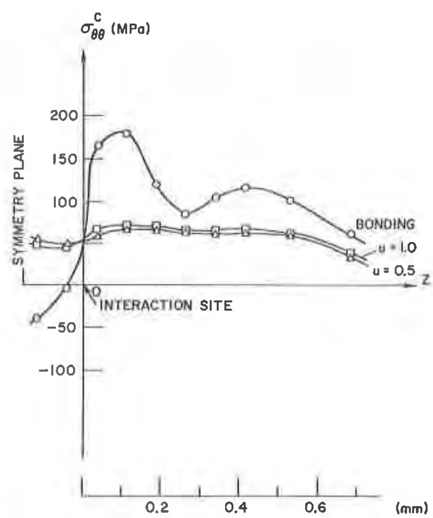

6. Comparison of cladding $\sigma_{\theta\theta}$ values under fuel-cladding bonding conditions and with two different friction coefficients. Stress values are at 1/4 of the cladding thickness, measured from the cladding inner surface. Neg. No. MSD-65953.